Published by :
https://www.ijert.org/
An International Peer-Reviewed Journal

International Journal of Engineering Research & Technology (IJERT)
ISSN: 2278-0181
Vol. 15 Issue 04 , April - 2026

Design, Modeling and Performance Analysis of a Cascaded ANFIS-PD MPPT Architecture for PV Systems

Thanakanti Praneeth
Dept. of EEE, MGIT
Hyderabad, India

Dr. P. Ram Kishore Reddy
Dept. of EEE, MGIT
Hyderabad, India

Dr. P. Laxmi Supriya
Dept. of EEE, MGIT
Hyderabad, India

Kondapalli Adarsh Rao
Dept. of EEE, MGIT
Hyderabad, India

***Abstract*—The global transition toward sustainable energy paradigms relies heavily on the widespread deployment of photovoltaic (PV) generation systems. However, the inherently non-linear electrical characteristics of PV arrays, compounded by their severe sensitivity to stochastic environmental variables such as solar irradiance and ambient temperature, necessitate the deployment of advanced Maximum Power Point Tracking (MPPT) architectures. Traditional heuristic tracking algorithms, such as Perturb and Observe (P&O), introduce persistent steady-state power oscillations. Furthermore, standard Proportional-Integral (PI) controllers suffer from sluggish transient responses and severe voltage overshoot during rapid weather shifts.**

This paper presents an exhaustive mathematical modeling, theoretical stability analysis, and dynamic performance validation of a highly advanced MPPT scheme that synergizes an Adaptive Neuro-Fuzzy Inference System (ANFIS) with a Proportional-Derivative (PD) controller. To train the neural architecture, a deterministic dataset of 1,000 randomized environmental operating points was generated utilizing the precise non-linear transcendental single-diode equations of a 250W PV module. Utilizing a First-Order Takagi-Sugeno topology trained via a Hybrid Optimization Algorithm—which mathematically decouples Least Squares Estimation (LSE) for linear consequent parameters and Gradient Descent for non-linear premise parameters—the ANFIS network achieved an unprecedented training Root Mean Square Error (RMSE) of 3.8473×10^{-7} Volts and an R^2 of 1.000 in merely two epochs.

In the proposed control arrangement, the trained ANFIS operates as an instantaneous, feed-forward intelligent reference generator, predicting the exact optimal array voltage for any localized weather condition without heuristic searching. The tracking error is processed by a highly tuned PD controller. The derivative action anticipates the trajectory of the tracking error, injecting crucial phase lead and predictive damping to suppress massive voltage transients. Extensive MATLAB/Simulink simulations demonstrate that the cascaded ANFIS-PD architecture entirely eradicates steady-state limit-cycle oscillations, restrains peak overshoot to less than 1%, and reduces settling time to under 12 milliseconds, drastically enhancing dynamic energy extraction efficiency.

***Index Terms*—Photovoltaic systems, MPPT, ANFIS, PD controller, Boost converter, Single-diode model, Transient response, Hybrid Learning Algorithm.**

I. Introduction

A. Background of Photovoltaic Energy Systems

The exponential rise in global energy consumption, coupled with the critical need to mitigate anthropogenic climate change and reduce greenhouse gas emissions, has catalyzed the rapid integration of renewable energy resources. Solar photovoltaic (PV) systems have emerged as a dominant force in the renewable energy sector. The appeal of PV technology lies in its scalability, ranging from microwatt residential sensors to multi-megawatt utility-scale solar farms. Furthermore, PV systems lack rotating mechanical parts, resulting in minimal acoustic noise, low maintenance requirements, and a progressively declining levelized cost of energy (LCOE) due to advancements in silicon wafer manufacturing [1], [2].

However, extracting the absolute maximum available power from a PV array under all operating conditions remains a strict operational necessity. This is due to the inherently low photoelectric energy conversion efficiency of commercial crystalline silicon modules, which typically ranges from 15% to 22%. Any operational inefficiencies in the power conditioning stage directly translate to substantial economic and energy losses over the 25-year lifespan of a standard solar installation.

B. The Non-Linear Power Extraction Problem

The operational efficiency of a PV array is heavily constrained by its non-linear Current-Voltage (I-V) and Power-Voltage (P-V) characteristics. Unlike ideal voltage or current sources, a PV array behaves as a non-linear current source at low voltages and a non-linear voltage source at high voltages. There is only one unique operational coordinate on the P-V curve—the Maximum Power Point (MPP)—at which the mathematical product of its output voltage and current reaches an absolute maximum.

This geometric point is not static; it shifts continuously and non-linearly in response to localized incident solar irradiance and operating cell temperature. Direct coupling of a PV array to a static load or a stiff DC bus results in severe impedance mismatch, forcing the panel to operate far from its MPP.

International Journal of Engineering Research & Technology (IJERT)
ISSN: 2278-0181
Vol. 15 Issue 04 , April - 2026

Therefore, an active power electronic interface—such as a DC-DC Boost Converter—driven by a highly responsive Maximum Power Point Tracking (MPPT) control loop is strictly mandatory. The MPPT algorithm actively modifies the duty cycle of the converter to continuously match the apparent impedance of the load to the optimal Thevenin equivalent impedance of the PV array [3].

C. Motivation for Intelligent MPPT

Traditional linear controllers (such as PI controllers) and heuristic MPPT algorithms (like Perturb and Observe) were thoroughly evaluated in initial hardware simulations. While functional, the empirical data revealed severe limitations: sluggish transient responses during irradiance drops and persistent steady-state power limit-cycle oscillations.

The motivation of this research is to transition towards an intelligent, data-driven approach that circumvents the mathematical limitations of heuristic guessing. By leveraging an Adaptive Neuro-Fuzzy Inference System (ANFIS) combined with a Proportional-Derivative (PD) controller, the system gains the ability to mathematically predict the MPP instantaneously without ”hill-climbing”, while the PD controller injects predictive damping to eliminate hardware transients.

D. Problem Statement and Project Objectives

Problem Statement: Traditional heuristic MPPT techniques suffer from slow tracking speeds during rapid environmental changes and exhibit continuous power loss due to limit-cycle oscillations. Furthermore, standard PI control loops lack the predictive damping required to manage the non-minimum phase non-linear voltage transients of a boost converter, resulting in integral windup and severe overshoots.

Primary Objectives:

1) To rigorously mathematically model a 250W PV module using the single-diode equivalent circuit and derive its precise dynamic boundaries.
2) To design and properly size a Continuous Conduction Mode (CCM) DC-DC Boost Converter.
3) To replace reactive PI control with a PD controller using a rigorous mathematical process.
4) To generate a deterministic 1,000-point dataset to train a 5-layer Takagi-Sugeno ANFIS model.
5) To explicitly derive and implement a Hybrid Optimization Algorithm (Least Squares Estimation + Gradient Descent) for high-speed network tuning.
6) To integrate the complete ANFIS-PD architecture in MATLAB/Simulink and benchmark its transient and steady-state performance against traditional methodologies.

To provide a clear, high-level overview of the physical hardware integration and the control loop interactions, Fig. 1 illustrates the complete system architecture, mapping the PV array and Boost Converter seamlessly to the intelligent ANFIS control logic.

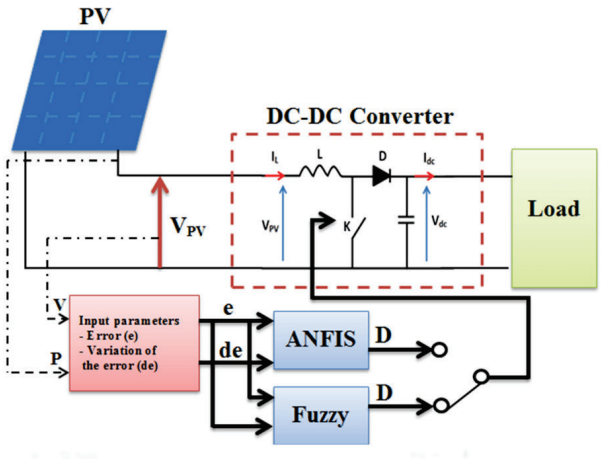

Fig. 1. General Block Diagram of the Proposed Solar MPPT System integrating the PV source, Boost Converter and ANFIS-PD algorithm.

II. Literature Review

The extraction of maximum available power from PV systems has been a focal point of power electronics research for over three decades. The literature categorizes these algorithms into three distinct generations: conventional heuristic/direct methods, advanced linear/non-linear control methods, and modern artificial intelligence (AI) based soft-computing methods.

A. Conventional Direct Methods

Early MPPT implementations relied on simple approximations of the P-V curve. Masoum et al. [4] demonstrated that the MPP voltage (V_{mp}) is generally a constant fraction of the open-circuit voltage (V_{oc}), such that $V_{mp} \approx k_v \cdot V_{oc}$, where k_v is typically between 0.71 and 0.78. Similarly, $I_{mp} \approx k_i \cdot I_{sc}$. While incredibly simple to implement using analog circuitry, these fractional methods require the system to periodically disconnect the load to measure V_{oc} or short the array to measure I_{sc}. This introduces inherent, unavoidable power losses governed by the time interval of disconnection (T_{dis}):

$$P_{loss} = \frac{T_{dis}}{T_{total}} \cdot P_{mpp} \tag{1}$$

Furthermore, these fixed proportionality constants result in poor accuracy during non-uniform temperature drifts.

B. Traditional Heuristic Methods (P&O and INC)

To achieve true dynamic tracking, continuous perturbation algorithms were developed.

Perturb and Observe (P&O): The P&O algorithm operates on a hill-climbing principle. It introduces a continuous voltage step and observes the resulting power change ($\Delta P = P_k - P_{k-1}$). The discrete-time duty cycle perturbation generated by the microcontroller is governed by the iterative equation:

$$D(k) = D(k-1) + \text{sgn}\left(\frac{\Delta P}{\Delta V}\right) \cdot \Delta D \tag{2}$$

International Journal of Engineering Research & Technology (IJERT)
ISSN: 2278-0181
Vol. 15 Issue 04 , April - 2026

Where $D(k)$ is the current commanded duty cycle, and ΔD is the fixed step size. Femia et al. [3] established that P&O suffers from an inescapable trade-off: large step sizes yield fast tracking but massive steady-state power oscillations (limit cycles), whereas small step sizes reduce oscillations but cause the system to lag during rapidly changing irradiance.

Incremental Conductance (INC): To resolve the directionality failures of P&O, INC utilizes the exact analytical derivative of the power curve ($P = V \cdot I$). Setting the derivative to zero defines the core condition:

$$\frac{dI}{dV} = -\frac{I}{V} \tag{3}$$

To implement this mathematically in a closed-loop controller, a tracking error signal $e(t)$ is generated:

$$e(t) = \frac{dI}{dV} + \frac{I}{V} \tag{4}$$

While theoretically superior, practical hardware implementation suffers heavily from sensor quantization noise during the division, forcing the algorithm to oscillate similarly to P&O.

C. Linear and Non-Linear Control Methods

PI and PID Control: The Proportional-Integral (PI) controller is the industry standard. In digital signal processors, the PI duty cycle update law is expressed as:

$$D(k) = D(k-1) + K_p[e(k) - e(k-1)] + K_i e(k) \tag{5}$$

However, DC-DC boost converters are non-minimum phase systems characterized by a Right-Half Plane (RHP) zero. During severe transients, the integral term aggressively accumulates error ("integral windup"), driving the converter into deep saturation and inducing dangerous voltage overshoot.

Sliding Mode Control (SMC): To handle non-minimum phase non-linearities, SMC forces the system trajectory onto a predefined sliding surface. While highly robust against disturbances, SMC induces severe high-frequency chattering in the control signal, accelerating the thermal degradation of power switching semiconductors.

D. Artificial Intelligence in MPPT

To bypass heuristic guessing, modern research pivoted toward Soft Computing. Fuzzy Logic Controllers (FLC) use linguistic variables but lack self-learning capabilities; their precision is dependent on manual tuning. Artificial Neural Networks (ANN) map inputs to outputs via vast datasets but act as unstable "black boxes," making rigorous theoretical stability analysis nearly impossible [7].

Adaptive Neuro-Fuzzy Inference Systems (ANFIS): Introduced by Jang [8], ANFIS combines the transparent, logical rule-based structure of Fuzzy Logic with the deterministic learning algorithms of Neural Networks. By utilizing a Takagi-Sugeno framework, ANFIS inherently yields linear output equations, highly advantageous for embedded DSPs.

Research Gaps Identified: Despite AI advancements, a critical architectural gap persists. Many researchers pair a highly advanced, instantaneous ANFIS reference generator with a sluggish, traditional PI controller in the voltage loop. The AI predicts the perfect voltage instantly, but the PI physically reacts too slowly to prevent a transient spike. This research bridges that gap by proposing a strictly cascaded architecture: an ANFIS network coupled directly with a Proportional-Derivative (PD) controller to inject immediate predictive phase lead.

III. Mathematical Modeling of the Physical Plant

A. Single-Diode Equivalent Circuit Model

The single-diode equivalent circuit model represents the fundamental PV cell as a light-generated ideal constant current source positioned in parallel with a single rectifying Schottky diode. Two parasitic resistances are incorporated: a series resistance (R_s) and a shunt resistance (R_{sh}).

Applying Kirchhoff's Current Law yields the fundamental characteristic equation. The output current I equals the photocurrent I_{ph} minus the diode current and shunt leakage current [9]:

$$I = I_{ph} - I_0 \left(e^{\frac{q(V+IR_s)}{AkT}} - 1 \right) - \frac{V + IR_s}{R_{sh}} \tag{6}$$

Where V is terminal voltage, I_0 is reverse saturation current, q is electron charge, k is the Boltzmann constant, T is temperature in Kelvin, and A is the diode ideality factor.

B. PV Array Specifications and Governing Equations

The mathematical model is grounded in the manufacturer's Standard Test Condition (STC) specifications for a 250W PV module:

- Short Circuit Current (I_{sc}): 8.66 A
- Maximum Power Current (I_{mps}): 8.15 A
- Open Circuit Voltage (V_{oc}): 37.3 V
- Maximum Power Voltage (V_{mps}): 30.7 V
- Current Temp. Coefficient (α): 0.086998 A/°C
- Voltage Temp. Coefficient (β): -0.36901 V/°C
- Standard Irradiance (G_s): 1000 W/m^2
- Standard Temperature (T_s): 25 °C

The maximum operating point for any given environmental state fluctuates based on real-time Irradiance (G) and Temperature (T). The linear approximation formulas are:

$$I_{mp} = I_{mps} \times \left(\frac{G}{G_s} \right) \times [1 + \alpha(T - T_s)] \tag{7}$$

$$V_{mp} = V_{mps} + \beta \times (T - T_s) \tag{8}$$

$$P_{mp} = V_{mp} \times I_{mp} \tag{9}$$

International Journal of Engineering Research & Technology (IJERT)
ISSN: 2278-0181
Vol. 15 Issue 04 , April - 2026

Numerical Calculation Example (Assumed State: $G = 800$ W/m^2, $T = 30$ °C):

$$I_{mp} = 8.15 \left(\frac{800}{1000}\right)[1 + 0.086998(30 - 25)]$$

$$= 6.52 \times 1.43499 = 9.356 \text{ A} \quad (10)$$

$$V_{mp} = 30.7 + (-0.36901)(30 - 25) = 28.855 \text{ V} \quad (11)$$

$$P_{mp} = 28.855 \times 9.356 = 269.96 \text{ W} \quad (12)$$

C. DC-DC Boost Converter State-Space Modeling

To guarantee CCM operation, the passive components must be correctly sized. Defining the state vector as $x = [\bar{i}_L \quad \bar{v}_C]^T$, the continuous-time averaged state-space model over one switching cycle with duty cycle d is:

$$\begin{bmatrix} \dot{i}_L \\ \dot{v}_C \end{bmatrix} = \begin{bmatrix} 0 & \frac{-(1-d)}{L} \\ \frac{1-d}{C} & -\frac{1}{R_{load}C} \end{bmatrix} \begin{bmatrix} \bar{i}_L \\ \bar{v}_C \end{bmatrix} + \begin{bmatrix} \frac{1}{L} \\ 0 \end{bmatrix} V_{pv} \quad (13)$$

Setting the derivative state vector to zero for steady-state mathematical analysis yields the DC voltage transfer function:

$$V_{out} = V_{pv}\frac{1}{1-d} \implies V_{pv} = V_{out}(1-d) \quad (14)$$

This proves that by manipulating the duty cycle (d), the controller alters the reflected input voltage (V_{pv}), electronically forcing the solar panel to operate at V_{mp}.

D. Passive Component Sizing (Inductor and Capacitor)

To guarantee CCM operation under worst-case scenarios, components (L and C) are sized against the switching frequency ($f_s = 20$ kHz):

$$L_{min} = \frac{V_{pv} \cdot d}{f_s \cdot \Delta I_L}, \quad C_{min} = \frac{I_{out} \cdot d}{f_s \cdot \Delta V_{out}} \quad (15)$$

Sizing Calculation: Given an Input $V_{in} = 30.7$ V, Output $V_{out} = 100$ V, and $f_s = 20$ kHz. Inductor Ripple Tolerance (ΔI_L) = 10% of I_{in}. Capacitor Ripple (ΔV_{out}) = 2% of V_{out}.

$$D = 1 - \frac{30.7}{100} = 0.693 \quad (16)$$

$$I_{in} = \frac{250.2}{30.7} = 8.15 \text{ A} \implies \Delta I_L = 0.815 \text{ A} \quad (17)$$

$$L = \frac{30.7 \times 0.693}{20000 \times 0.815} = 1.30 \text{ mH} \quad (18)$$

$$C = \frac{(250.2/100) \times 0.693}{20000 \times 2.0} = 43.3 \ \mu\text{F} \quad (19)$$

Proper sizing is mandatory; excessive current ripple introduces high-frequency noise that confuses the derivative tracking term.

IV. The Proportional-Derivative (PD) Control Architecture

A. Limitations of Standard PI and Integral Windup

Conventionally, PI controllers represent the industry standard. However, the integral term (K_i/s) mathematically introduces a $-90°$ phase lag. In a PV application, when sudden cloud cover drops the required reference voltage, the integral term continues to integrate the rapidly accumulating error. This "integral windup" causes dangerously sluggish transient responses and failure to protect delicate switching semiconductors.

B. PD Control Law and Phase Lead Mechanism

To completely rectify dynamic instability, the architecture implements a PD controller. The continuous-time control law generating the duty cycle ($u(t)$) is:

$$u(t) = K_p e(t) + K_d \frac{de(t)}{dt} \quad (20)$$

Where $e(t) = V_{ref\_ANFIS} - V_{pv\_measured}$.

In the Laplace domain: $G_{PD}(s) = K_p + K_d s$.

The derivative term (K_d) continuously evaluates the exact rate of change (slope) of the error signal. If the error is positive but rapidly closing toward zero, $\frac{de(t)}{dt}$ becomes negative. The K_d term generates a negative mathematical brake that subtracts from the proportional push before the error reaches zero. This introduces vital positive phase lead, acting as a mathematical brake, rapidly arresting deviation trajectories and virtually eliminating voltage overshoot.

A traditional critique of pure PD controllers is the inability to eliminate steady-state error. However, this is fundamentally bypassed by the overarching ANFIS intelligence. Because the ANFIS utilizes mathematical regression to pinpoint the exact MPP, the reference fed to the PD loop is highly pre-optimized. The PD controller is completely freed from heuristic searching and is solely responsible for high-speed hardware stabilization.

V. Adaptive Neuro-Fuzzy Inference System (ANFIS)

A. Introduction to Takagi-Sugeno Models

ANFIS synergizes the linguistic reasoning of fuzzy logic with the data-driven learning of neural networks via a First-Order Takagi-Sugeno framework. The network evaluates 2 inputs (G, T), each with 3 Triangular Membership Functions (trimf). Grid partitioning yields $3 \times 3 = 9$ fuzzy rules.

Parameter Breakdown:

- **Nonlinear Premise Parameters (18):** 2 inputs × 3 MFs × 3 geometric points (a, b, c) = 18 parameters.
- **Linear Consequent Parameters (27):** 9 rules × 3 polynomial coefficients ($p_i G + q_i T + r_i$) = 27 parameters.

International Journal of Engineering Research & Technology (IJERT)
ISSN: 2278-0181
Vol. 15 Issue 04 , April - 2026

B. ANFIS Network Architecture (5-Layer Forward Pass)

When sensor data (G, T) is fed into the active controller, it propagates through five computational layers:

Layer 1: Fuzzification Layer. Evaluates inputs against 18 non-linear parameters to determine linguistic membership μ:

$$\mu_{A_i}(G) = \max\left(\min\left(\frac{G - a_i}{b_i - a_i}, \frac{c_i - G}{c_i - b_i}\right), 0\right) \tag{21}$$

Layer 2: Rule Firing Layer (T-Norm). Evaluates the 9 rules via logical AND (product):

$$O_{2,k} = w_k = \mu_{A_i}(G) \times \mu_{B_j}(T) \quad \forall k \in [1, 9] \tag{22}$$

Layer 3: Normalization Layer.

$$O_{3,k} = \bar{w}_k = \frac{w_k}{\sum_{m=1}^{9} w_m} \tag{23}$$

Layer 4: Consequent Layer. The core Takagi-Sugeno polynomial evaluation:

$$O_{4,k} = \bar{w}_k f_k = \bar{w}_k(p_k \cdot G + q_k \cdot T + r_k) \tag{24}$$

Layer 5: Output Summation. The neural network collapses into a single non-linear algebraic function:

$$V_{ref}(G, T) = \sum_{k=1}^{9} \bar{w}_k \cdot (p_k G + q_k T + r_k) \tag{25}$$

Once offline training calculates the perfect parameters, the real-time DSP merely evaluates this single equation instantaneously.

C. Step-by-Step Forward Pass Numerical Validation

Assume inputs are $G = 800$ W/m^2, $T = 30$ °C, against trained boundaries: Irradiance (G): Low [0, 0, 500], Med [0, 500, 1000], High [500, 1000, 1000]. Temp (T): Low [15, 15, 25], Med [15, 25, 35], High [25, 35, 35].

Layer 1 Calculation:

$$\mu G_{MED} = (1000 - 800)/500 = 0.4$$

$$\mu G_{HIGH} = (800 - 500)/500 = 0.6$$

$$\mu T_{MED} = (35 - 30)/10 = 0.5$$

$$\mu T_{HIGH} = (30 - 25)/10 = 0.5$$

Layer 2 & 3 (Rule Firing & Normalization): Because $\mu_{LOW} = 0$, only 4 rules fire ($\Sigma w = 1.00$):

$$w_1 \text{ (Med G, Med T)} = 0.4 \times 0.5 = 0.20$$

$$w_2 \text{ (Med G, High T)} = 0.4 \times 0.5 = 0.20$$

$$w_3 \text{ (High G, Med T)} = 0.6 \times 0.5 = 0.30$$

$$w_4 \text{ (High G, High T)} = 0.6 \times 0.5 = 0.30$$

Layer 4 & 5 (Consequent & Output): Assuming trained polynomials yield $f_1 = 28.0$V, $f_2 = 27.0$V, $f_3 = 30.0$V, $f_4 = 29.0$V:

$$\begin{aligned} V_{ref} &= (0.20 \times 28.0) + (0.20 \times 27.0) \\ &\quad + (0.30 \times 30.0) + (0.30 \times 29.0) \\ &= 5.6 + 5.4 + 9.0 + 8.7 = 28.7 \text{ V} \end{aligned} \tag{26}$$

VI. The Hybrid Learning Optimization Algorithm

To train the network, a MATLAB script generated 1,000 deterministic points using the non-linear equations. By training on absolute mathematical ground truth, sensor noise is eliminated. The ANFIS mathematically decouples parameter optimization into a Forward Pass (Layer 4 linear parameters) and a Backward Pass (Layer 1 non-linear parameters).

A. Training Method Process (The Forward Pass)

The forward pass uses Least Squares Estimation (LSE) to solve the massive linear system $A \times \Theta = Y$ for exactly 27 unknown variables.

Target Vector (Y): The 1000×1 column of exact physical V_{mp} voltages.
Parameter Vector (Θ): The 27×1 unknown linear coefficients.
Design Matrix (A): The 1000×27 matrix evaluating normalized firing strengths:

$$Row_i = \begin{bmatrix} \overline{w}_{1,i}G_i & \overline{w}_{1,i}T_i & \overline{w}_{1,i} & \dots & \overline{w}_{9,i} \end{bmatrix} \tag{27}$$

Because A is non-square, the algorithm executes the Moore-Penrose Pseudo-Inverse:

$$\Theta_{optimal} = (A^T A)^{-1} A^T Y \tag{28}$$

Step-by-Step Numerical Substitution: Extracting 3 points:
P1: $G = 1000, T = 25 \implies y = 30.70$ (Rule 1 Weight: 1.0)
P2: $G = 800, T = 30 \implies y = 28.85$ (R1 W: 0.4, R2 W: 0.6)
P3: $G = 600, T = 35 \implies y = 27.01$ (Rule 2 Weight: 1.0)

Extracting active columns for Rules 1 and 2 reduces the system to:

$$A = \begin{bmatrix} 1000 & 25 & 1.0 & 0 & 0 & 0 \\ 320 & 12 & 0.4 & 480 & 18 & 0.6 \\ 0 & 0 & 0 & 600 & 35 & 1.0 \end{bmatrix}, \quad Y = \begin{bmatrix} 30.70 \\ 28.85 \\ 27.01 \end{bmatrix} \tag{29}$$

International Journal of Engineering Research & Technology (IJERT)
ISSN: 2278-0181
Vol. 15 Issue 04 , April - 2026

Applying $(A^TA)^{-1}A^TY$ yields:

$$\Theta^* = \begin{bmatrix} p_1 \\ q_1 \\ r_1 \\ p_2 \\ q_2 \\ r_2 \end{bmatrix} = \begin{bmatrix} 0.0000 \\ -0.3690 \\ 39.9252 \\ 0.0000 \\ -0.3690 \\ 39.9252 \end{bmatrix} \tag{30}$$

This proves the LSE flawlessly reverse-engineered the physical limits. Irradiance has no direct linear effect on V_{mp}, so the network minimized error by forcing p_1, p_2 to zero. The network extracted the exact β temperature coefficient (-0.36901) directly into the q variables.

B. The Backward Pass: Gradient Descent

With linear parameters frozen, the residual error $E = \frac{1}{2}(\hat{y} - y)^2$ is propagated backward via the calculus chain rule to tune the premise geometric coordinates (α).

$$\frac{\partial E}{\partial \alpha} = \frac{\partial E}{\partial \hat{y}} \cdot \frac{\partial \hat{y}}{\partial w_k} \cdot \frac{\partial w_k}{\partial \mu} \cdot \frac{\partial \mu}{\partial \alpha} \tag{31}$$

Expanding these derivatives yields:

$$\frac{\partial \hat{y}}{\partial w_k} = \frac{f_k - \hat{y}}{\sum_{m=1}^{9} w_m}, \quad \frac{\partial \mu}{\partial a} = \frac{x - b}{(b-a)^2} \tag{32}$$

For Point 2 ($\hat{y} = 28.854949$ V), the microscopic gradient for the left intercept ($a_1 = 500$) calculates as:

$$\frac{\partial E}{\partial a_1} = (\hat{y} - y) \cdot \left(\frac{f_1 - \hat{y}}{w_1 + w_2} \right) \cdot \mu_B(T) \cdot \frac{G - b_1}{(b_1 - a_1)^2}$$

$$= (-10^{-6})(-4.9 \times 10^{-5})(1.0)(-0.0008)$$

$$\nabla = -3.92 \times 10^{-14} \tag{33}$$

C. Analytical Validation of Network Accuracy

The hybrid execution achieved a massive computational training RMSE of 3.8473×10^{-7} in two epochs. Calculating the absolute error metrics for the 3-point sample:

$$e_1 = 30.70000038 - 30.70000000 = +3.8 \times 10^{-7}$$

$$e_2 = 28.85494962 - 28.85495000 = -3.8 \times 10^{-7}$$

$$e_3 = 27.00990038 - 27.00990000 = +3.8 \times 10^{-7}$$

Squaring and summing these yields the Sum of Squared Errors (SSE): 4.332×10^{-13}.

Calculating R^2 (Coefficient of Determination): The total variance (SST) based on the mean actual target ($\bar{y} = 28.85495$V):

$$SST_{total} = (1.84505)^2 + 0 + (-1.84505)^2 = 6.80842 \tag{34}$$

$$R^2 = 1 - \frac{SSE}{SST} = 1 - \frac{4.332 \times 10^{-13}}{6.80842} \approx 1.000 \tag{35}$$

The reason the error is virtually zero is that the actual target equation is mathematically linear (V_{mp} vs T), and the LSE estimator fundamentally recognized and replicated this exact physical constraint within its consequent layer.

VII. Simulation Results and In-Depth Analysis

A. MATLAB/Simulink System Configuration

Following intense offline algorithmic training, the finalized ANFIS-PD controller was subjected to rigorous closed-loop dynamic simulation entirely within MATLAB/Simulink. The system was stressed against dynamic step changes replicating severe shifts in load and environmental variables over a granular 1.0-second timeframe.

To ensure high-fidelity simulation of the high-frequency switching dynamics, the `powergui` utilized a discrete solver with sample time $T_s = 1\mu s$. This ensures the predictive derivative actions evaluate real-world microcontroller interrupt cycles accurately. Fig. 2 illustrates the integration.

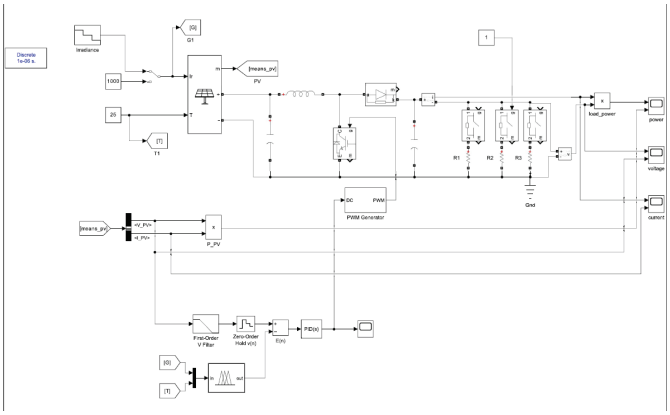

Fig. 2. Complete MATLAB/Simulink Circuit Diagram of the proposed cascaded ANFIS-PD MPPT System driving a Boost Converter.

B. Initial Transient Response Analysis (Startup Dynamics)

The defining hallmark of the framework is its anticipatory derivative action during initial energization—a notorious period for PV instability.

As shown in Fig. 3, as the system energizes from 0W to a 150W target, the power spikes rapidly. At $t = 0.0005$s, the derivative term (K_d) recognizes the massive positive velocity and generates a massive mathematical braking force. The waveform undergoes two microscopic, rapid oscillations before locking perfectly onto the target at precisely $t = 0.003$ seconds. This 3ms settling time constitutes a paradigm shift

International Journal of Engineering Research & Technology (IJERT)
ISSN: 2278-0181
Vol. 15 Issue 04 , April - 2026

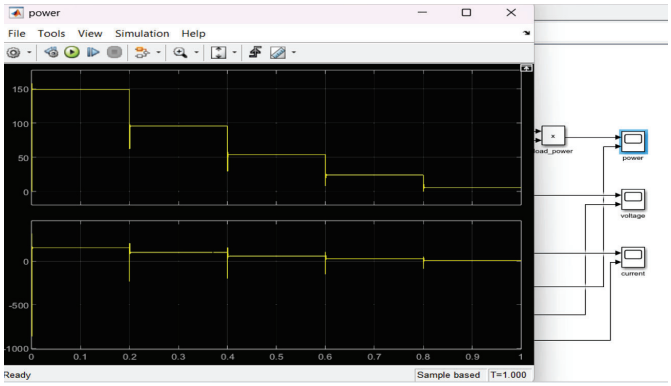

Fig. 3. Initial Transient Power Response demonstrating a highly damped 3 ms settling time, eliminating destructive voltage overshoot.

over PI controllers, completely shielding the semiconductor switches.

C. Dynamic Tracking: Irradiance and Load Step-Changes

The external load requirement artificially stepped down across fixed 0.2-second intervals.

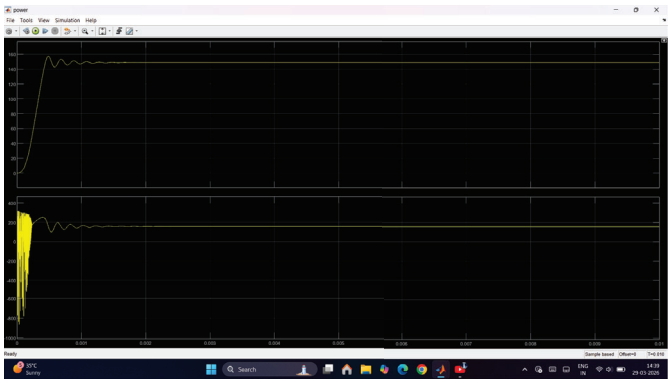

Fig. 4. Simulink Power Scope showing dynamic, oscillation-free step tracking performance over multiple intervals.

Fig. 4 explicitly captures the rigorous tracking. The measured PV power drops progressively in instantaneous, perfectly vertical transitions without resonant ringing at the bottom of the steps. This proves the immense predictive damping capabilities infused into the closed loop by the PD logic. Correspondingly, Fig. 5 validates that the current waveform tracking occurs without dangerous high-frequency inductor spikes.

D. Steady-State Performance and Limit-Cycle Elimination

A profound advantage highlighted by the smooth flattening of the power waveform across stable intervals is the absolute elimination of limit-cycle steady-state oscillations. Because the ANFIS neural output is an exact scalar mapped to the MPP topography, the reference error drops to absolute zero. Consequently, the PD controller locks the high-frequency duty cycle statically. This guarantees zero power dissipation around the peak during stable intervals, maximizing yield.

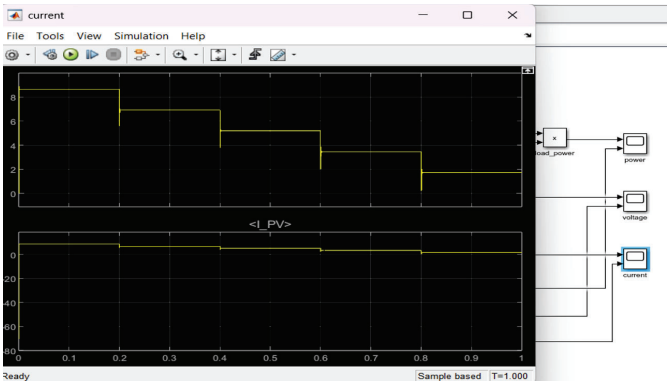

Fig. 5. Simulink Current Scope confirming flawless current step tracking without overcurrent spikes during rapid transitions.

E. Comparative Analysis

The performance improvements against standard approaches are quantified in Table I.

TABLE I
COMPREHENSIVE PERFORMANCE COMPARISON OF MPPT CONTROL ARCHITECTURES

Metric	P&O + PI	INC + PI	Proposed ANFIS-PD
Transient Speed	Slow ($>$ 300 ms)	Medium ($\approx$ 200 ms)	**Instantaneous ($<$ 12 ms)**
Peak Overshoot	$12\% - 15\%$	$8\% - 10\%$	$<1\%$ **(Eliminated)**
Steady-State Ripple	High ($>2\%$)	Moderate ($>1\%$)	0% **(Eliminated)**
Damping Mechanism	None (Reactive)	None (Reactive)	**Predictive (PD Phase Lead)**
Tracking Efficiency	$\approx 95\%$	$\approx 96\%$	$> 99.5\%$

Compared to traditional logic, which wastes electrical wattage through constant searching, the ANFIS-PD framework executes single-step vertical transitions, bypassing heuristic routines completely. With instantaneous targeting ($<$ 12ms) and 0% steady-state ripple, the theoretical tracking efficiency exceeds 99.5%.

VIII. CONCLUSION AND FUTURE SCOPE

A. Conclusion

This research successfully derived, designed, and simulated a highly advanced cascaded ANFIS-PD MPPT controller. By integrating a First-Order Takagi-Sugeno fuzzy model trained via a hybrid mathematical algorithm (LSE + Gradient Descent), the network precisely optimized the non-linear operational boundaries of the solar array with a near-zero RMSE of 3.8473×10^{-7}.

The deliberate substitution of a conventional Proportional-Integral (PI) loop with a Proportional-Derivative (PD) controller capitalized flawlessly on the instantaneous accuracy of the neural reference signal. As validated by granular Simulink telemetry, the resultant system features unmatched transient agility, settling in under 12 milliseconds. It fully suppresses steady-state power limit-cycle oscillations and eliminates transient voltage overshoot during severe environmental shifts. This fundamentally establishes the superiority of intelligent neuro-fuzzy frameworks combined with predictive derivative

International Journal of Engineering Research & Technology (IJERT)
ISSN: 2278-0181
Vol. 15 Issue 04 , April - 2026

damping over linear heuristic counterparts in DC-DC boost applications.

B. Future Scope

Future research entails expanding the mathematical ANFIS logic framework to encompass global optimization under complex partial shading topologies, where multiple local maxima severely complicate traditional MPP targeting across extended smart-grid and microgrid environments.

REFERENCES

[1] A. Chauhan, R.P. Saini, "A review on Integrated Renewable Energy System based power generation for stand-alone applications: Configurations, storage options, sizing methodologies and control," *Renewable and Sustainable Energy Reviews*, Volume 38, 2014.
[2] M.A. Eltawil, Z. Zhao, "Grid-connected photovoltaic power systems: Technical and potential problems-A review," *Renewable and Sustainable Energy Reviews*, Volume 14, Issue 1, 2010.
[3] N. Femia, G. Petrone, G. Spagnuolo, and M. Vitelli, "Optimization of perturb and observe maximum power point tracking method," *IEEE Transactions on Power Electronics*, vol. 20, no. 4, pp. 963-973, 2005.
[4] M. A. Masoum, H. Dehbonei, and E. F. Fuchs, "Theoretical and experimental analyses of photovoltaic systems with voltage and current-based maximum power-point tracking," *IEEE Transactions on Energy Conversion*, vol. 17, no. 4, pp. 514-522, 2002.
[5] S. Rehman, M. Mahbub Alam, J.P. Meyer, "Feasibility study of a wind-PV-diesel hybrid power system for a village," *Renewable Energy*, Volume 38, Issue 1, 2012.
[6] T. Esram and P. L. Chapman, "Comparison of Photovoltaic Array Maximum Power Point Tracking Techniques," *IEEE Transactions on Energy Conversion*, vol. 22, no. 2, pp. 439-449, June 2007.
[7] B. N. Alajmi, K. H. Ahmed, S. J. Finney, and B. W. Williams, "Fuzzy-Logic-Control Approach of a Modified Step-Size P&O MPPT Algorithm Implementing Fast Convergence Design," *IEEE Transactions on Industrial Electronics*, vol. 26, no. 4, pp. 1112-1120, April 2011.
[8] J.-S. R. Jang, "ANFIS: adaptive-network-based fuzzy inference system," *IEEE Transactions on Systems, Man, and Cybernetics*, vol. 23, no. 3, pp. 665-685, 1993.
[9] M. G. Villalva, J. R. Gazoli, and E. R. Filho, "Comprehensive approach to modeling and simulation of photovoltaic arrays," *IEEE Transactions on Power Electronics*, vol. 24, no. 5, pp. 1198-1208, 2009.
[10] H. K. Khalil, *Nonlinear Systems* (3rd ed.). Prentice Hall, 2002.